This is a peer-reviewed, author's accepted manuscript of the following conference proceedings article:
Aburaed, N., Alkhatib, M. Q., Marshall, S., Zabalza, J., & Ahmad, H. A. (2023).
Complex-valued neural network for hyperspectral single image super resolution. In N. J. Barnett (Ed.),
Proc. SPIE 12338, Hyperspectral Imaging and Applications II (Vol. 12338). (Proc. of SPIE). SPIE. https://doi.org/10.1117/12.2645086

Complex-valued Neural Network for Hyperspectral Single Image Super Resolution

Nour Aburaed[a,b], Mohammed Q. Alkhatib[b], Stephen Marshall[a], Jaime Zabalza[a], and Hussain Al Ahmad[b]

[a]Department of Electronic and Electrical Engineering, University of Strathclyde, Glasgow, UK
[b]College of Engineering and IT, University of Dubai, Dubai, UAE

ABSTRACT

Remote sensing applications are nowadays widely spread in various industrial fields, such as mineral and water exploration, geo-structural mapping, and natural hazards analysis. These applications require that the performance of image processing tasks, such as segmentation, object detection, and classification, to be of high accuracy. This can be achieved with relative ease if the given image has high spatial resolution as well as high spectral resolution. However, due to sensor limitations, spatial and spectral resolutions have an inherently inverse relationship and cannot be achieved simultaneously. Hyperspectral Images (HSI) have high spectral resolution, but suffer from low spatial resolution, which hinders utilizing them to their full potential. One of the most widely used approaches to enhance spatial resolution is Single Image Super Resolution (SISR) techniques. In the recent years, Deep Convolutional Neural Networks (DCNNs) have been widely used for HSI enhancement, as they have shown superiority over other traditional methods. Nonetheless, researches still aspire to enhance HSI quality further while overcoming common challenges, such as spectral distortions. Research has shown that properties of natural images can be easily captured using complex numbers. However, this has not been thoroughly investigated from the perspective of HSI SISR. In this paper, we propose a variation of a Complex Valued Neural Network (CVNN) architecture for HSI spatial enhancement. The benefits of approaching the problem from a frequency domain perspective will be answered and the proposed network will be compared to its real counterpart and other state-of-the-art approaches. The evaluation and comparison will be recorded qualitatively by visual comparison, and quantitatively using Peak Signal-to-Noise Ratio (PSNR), Structural Similarity Index (SSIM), and Spectral Angle Mapper (SAM). The project can be accessed at: https://github.com/NourO93/3D_CCVNN_Hyperspectral

Keywords: Hyperspectral, spatial enhancement, super resolution, single image super resolution, complex valued neural networks, CNN, 3D-CNN

1. INTRODUCTION

Enhancing images in general and remote sensing imagery in particular has been a popular problem in the literature ever since the 1980s. Efforts have been exerted to enhance Panchromatic (PAN), RGB, and other Multispectral Images (MSI).[1–4] This problem is even more interesting when it comes to Hyperspectral Images (HSI) because their spatial resolution is considerably lower than MSI. In the literature, spatial enhancement of HSI methods are split into two categories; Fusion and Single Image Super Resolution (SISR). Fusion is the process of combining two or more images, such that the product reveals more information than each individual image. In this case, the combined images are HSI with MSI, RGB, or PAN, such that the resulting image has high spectral resolution and high spatial resolution simultaneously. Fusion methods have been widely used since the late 1990s.[5] Their success has been demonstrated in several studies that can be grouped into: Component Substitution,[6] Multi-resolution Analysis,[7] Matrix Factorization,[8] Tenosr-based,[9–11] Bayesian-based,[12] and Deep Convolutional Neural Networks (DCNNs).[13–18] The main advantage of Fusion methods is the ability to enhance the spatial quality of HSI beyond a scale factor of 8 with minimal spectral distortions. On the other hand, the main disadvantages include high computational complexity and impracticality when auxiliary information are unavailable. For instance, capturing MSI and HSI of the same scene with precise co-registration is considered as

Further author information:
N. A.: E-mail: nour.aburaed@ieee.org

an impractical assumption. Additionally, most methods require knowledge about the sensor, such as its Point Spread Function (PSF), which makes them inapplicable in scenarios where such information is unattainable. As for the other category, SISR, it is the process of constructing a High Resolution (HR) image from a single Low Resolution (LR) counterpart. SISR research studies can be grouped into: interpolation, regularization, Super Resolution Mapping (SRM), and DCNNs. SISR methods do not require an auxiliary image, which offers flexibility and convenience with regards to implementation. However, this is a double-edged sword, as it makes SISR a highly ill-posed problem, and it is challenging to upscale an image beyond a scale factor of 8.

In both Fusion and SISR fields of research, DCNN approaches show superiority against other traditional approaches thanks to their ability to overcome certain challenges, such as spectral distortions and co-registration requirement. Nonetheless, DCNNs present a new set of problems. For instance, models that follow supervised learning scheme exhibit poor performance when the size of the training dataset is limited. Additionally, DCNN models usually perform well on datasets captured by certain sensors, but not necessarily on others. Therefore, scientists constantly strive to boost the performance of existing HSI-SR approaches while overcoming spectral distortions. Evidence suggests that processing images in the frequency domain offers direct access to high and low frequency components, allowing direct manipulation of these parameters and, in turn, easier construction of intrinsic image details, such as sharp edges. The branch of neural networks that is capable of manipulating complex inputs is referred to as Complex-Valued Neural Networks (CVNNs). Using this type of network for the purpose of HSI SISR has not been attempted thus far.

In this paper, a preliminary study on the effectiveness of CVNNs at enhancing the spatial quality of HSI through SISR is conducted. In particular, a 3D Convolutional CVNN (3D-CCVNN) is implemented, trained, and tested using the publicly available HSI datasets, Botswana[19] and Pavia University (PU).[19] The performance of the network is evaluated and compared against other state-of-the-art approaches using Peak Signal-to-Noise Ratio (PSNR), Structural Similarity Index Measurement (SSIM), and Spectral Angle Mapper (SAM). The quality of the enhanced images is also compared qualitatively by visual inspection and by plotting spectral signature. The rest of the paper is organized as follows: Section 2 discusses the related work, Section 3 demonstrates the mathematical background behind the problem and the proposed methodology, Section 4 illustrates and analyzes the results, and finally, Section 5 summarizes the paper and states the future direction of this research.

2. RELATED WORK

The approach presented in this paper is related to SISR. Therefore, only SISR background will be discussed in this section, as Fusion approaches are out of this scope. SISR is considered as a mapping problem between an HR-HSI and its corresponding LR-HSI. Due to the non-linear nature of DCNNs and their capability to extract features automatically without the need for hand-crafted features, they can facilitate an end-to-end mapping between both images. DCNNs operations, such as convolution and pooling, can be two-dimensional (2D) or three-dimensional (3D). In 2017,[20] it has been demonstrated that 3D operations are better suited for processing HSI, as they preserve the spectral signature by processing the HSI cube as a whole rather than processing it band-by-band. 3D Full Convolutional Neural Network (3D-FCNN) follows this principle and inspired a lot of studies afterwords to follow suit. For example, the authors in[21] expanded the traditional 2D Super Resolution CNN (SRCNN) to 3D and adjusted its filter sizes to enhance HSI. They show that by unifying filter sizes, the network produces less artifacts around the edges. Additionally, the network does not need large computational resources and performs better than its 2D counterpart as well as 3D-FCNN. In another study, an encoder-decoder architecture design inspired by 2D-UNET[2] was also utilized to enhance HSI spatially.[22] The proposed network exhibits two symmetrical sides, where the encoder extracts features through a series of 3D convolution and pooling, and the decoder side reconstructs the target enhanced HSI by inverting these operations in 3D as well. Furthermore, there are internal residual connections between encoder units and decoder units, as well as external residual connections across encoders and decoders to improve information exchange between the layers. This network is dubbed 3D Residual UNET (3D-RUNET).[22] The literature is rich with other similar examples.[23–26]

All the aforementioned DCNNs process HSI in the spatial domain. Enhancing HSI using CVNNs is an approach that has not been explored thus far, and it has the potential to further boost the performance of HSI enhancement techniques. The next section explains the mathematical framework of the problem and the proposed approach, which will make the advantage of CVNNs more apparent.

3. MATHEMATICAL FRAMEWORK

3.1 Problem Statement

The mapping between a real-valued LR-HSI denoted X_r and a real-valued, ground truth HR-HSI denoted Y_r can be mathematically formulated using Equation 1.

$$X_r = DGY_r + \mathcal{E}, \tag{1}$$

where D is the downsampling operation, G is the blurring filter, and $\mathcal{E}$ is the additive noise. The goal is to find $\hat{Y}_r$, such that the Error between X_r and DGY_r is miminal. This error can be estimated using various functions. This study utilizes the standard Mean Squared Error (MSE).

In order to generate X_r, nearest neighbor interpolation is used as a downsampling operation, and Gaussian blur is used as a blurring filter. To simplify the study, the additive noise is considered negligible. This is a commonly accepted approach in the literature for generating LR-HSI.[24]

3.2 Proposed Methodology (3D-CCVNN)

The interest in CVNNs has been increasing due to the natural statistical correlation that occurs between the real and imaginary parts of complex numbers in signals. This correlation applies to HSI as well.[27] As mentioned in Section 2, 3D convolution operations are more suited for processing HSI than 2D. To implement the complex domain counterpart of a conventional real-valued 3D convolution, each band of the HSI cube must be converted to the complex domain and convolved with a complex filter. In this study, Band-wise Fast Fourier Transform (FFT) is used for this purpose. For a complex HSI cube denoted $X = [X_r + iX_{im}]$, and a Kernel denoted $K = [K_r + iK_{im}]$, where $X_r, X_{im}, K_r, K_{im} \in \mathbb{R}$, a 3D Complex Convolutional (CC) layer is defined using the following equation:

$$F_{(x,y,z)} = iReLU\left(\sum_{i=1}^{M}\sum_{j=1}^{M}\sum_{k=1}^{C} K_{(i,j,k)}X_{(x+i,y+j,z+k)} + b\right), \tag{2}$$

where iReLU, which stands for imaginary Rectified Linear activation Unit, is a complex activation function defined as $max(0, z)$ for some $z \in \mathbb{C}$, and b is the complex bias. The output F is then passed to a similar CC layer, which is in turn passed to another similar layer, and then finally the last CC layer that gives the final output. At this stage, F is converted back to a real signal using band-wise Inverse FFT (IFFT). The loss function used in this research is a standard MSE loss function. Hence, the loss function is real-valued, but the weights are complex. The overall architecture of the proposed 3D-CCVNN model is illustrated in Figure 1. The number of filters and kernel sizes are indicated in the figure, and they have been chosen in a way that imitates the 3D-SRCNN, since its filter and kernel sizes have already proven efficiency in removing artifacts around the borders of the image. Since the 3D-CCVNN is not very deep, pooling and batch normalization layers have been avoided. Additionally, a residual connection was added to boost the performance, as it has been proven that residual connection enhance SISR training.[28]

4. EXPERIMENTAL RESULTS

4.1 Datasets

The first dataset used in this study is Botswana.[19] It was captured using Hyperion sensor onboard the NASA EO-1 satellite over the Okavango Delta, Botswana. The spatial resolution is 30m, with 242 bands that cover 400-2500nm portion of the spectrum in 10nm intervals. Some bands were corrupted due to water absorption and were thus removed. The remaining number of bands is 145. THe total number of pixels in Botswana scene is 1467×256.

The second dataset used in this study is PU.[19] This dataset was captured using Reflective Optics System Imaging Spectrometer (ROSIS) sensor over Pavia, Italy. it consists of 115 bands, and the number goes down

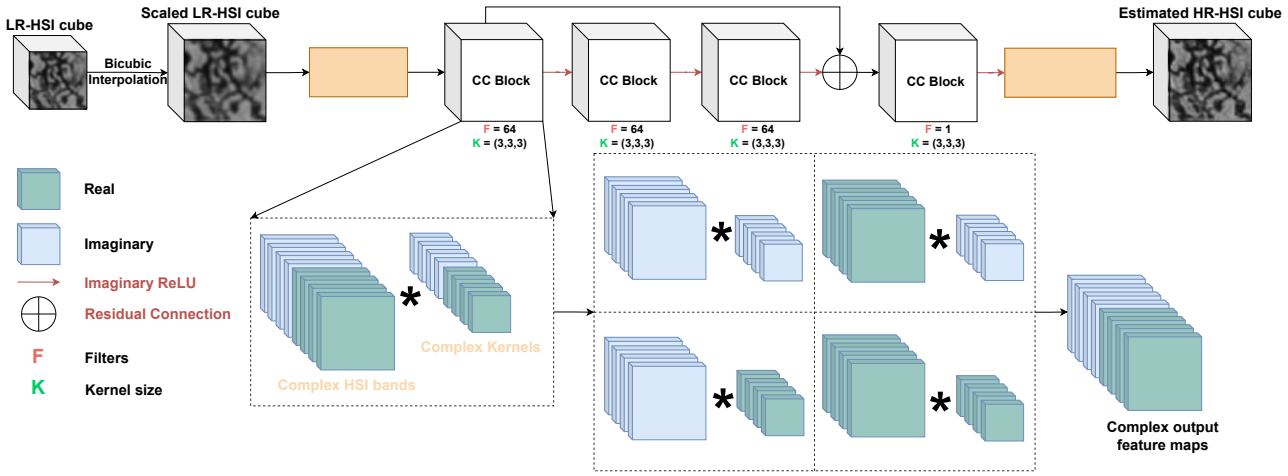

Figure 1. Overall architecture of the proposed 3D-CCVNN.

to 103 after removing the corrupted ones. It covers the spectrum from 430-960nm in 10nm interval. The total number of pixels is 610×340.

Each dataset was divided into patches of 64×64. Approximately 83% of the patches were used for training, and the remaining were used for testing and validation. Table 1 summarizes the characteristics of each dataset and the resulting number of patches.

Table 1. Characteristics of the datasets used in this study; Botswana and PU.

Dataset	Sensor	# of bands	Spectral range (nm)	Spatial resolution (m)	# of patches		
					Training	Testing	Validation
Botswana[19]	Hyperion	145	400-2500	30	76	8	8
PU[19]	ROSIS	103	430-960	1.3	37	4	4

4.2 Evaluation and Analysis

The proposed 3D-CCVNN was built, trained, and tested using Tensorflow library. The training parameters indicate 100 epochs and MSE as a loss function. The networks used for comparison, namely 3D-FCNN, 3D-SRCNN, and 3D-RUNET were all trained using the same environment and parameters to ensure fairness.

The quantitative results of Botswana dataset are shown in Table 2 for scale factors $\times 2$ and $\times 4$. The results indicate that the 3D-CCVNN prevails over every other method in terms of PSNR and SAM. Despite the clear improvement in PSNR and SAM, it appears that this is not the case for SSIM, as 3D-CCVNN sometimes achieves only slightly better SSIM than other methods, or slightly worse. This could be attributed to the simplicity of the network. Since 3D-CCVNN is not deep and it consisted of only 3D CC layers, this might have impacted the reconstruction of grayscale levels in each band. Figure 2 shows the predictions of HR-HSI from each method using Botswana dataset. 3D-CVNN shows the closest visual quality to the ground truth. Although 3D-CCVNN and 3D-RUNET appear visually similar, their MSE map shows that 3D-CCVNN exhibits less errors and less blurriness compared to 3D-RUNET. The spectral signature plotted in Figure 3 reveals that 3D-CCVNN follows the spectral signature of the ground truth more closely compared to other methods, which is consistent with SAM results in Table 2.

PU dataset results are shown in Table 3. Since the dataset size of PU is smaller than that of Botswana, the results for the former are overall inferior to the latter. This is true for all methodologies demonstrated. In this dataset's case, 3D-CCVNN prevails in terms of PSNR and SSIM. The SAM produced by 3D-CCVNN is superior to that of bicubic interpolation and 3D-FCNN, but it falls behind 3D-SRCNN and 3D-RUNET. Figure 4 shows visual results of the estimated HR-HSI as predicted by each method. It can be observed that the 3D-CCVNN is the closest to the ground truth, especially when comparing the error map produced by each

Table 2. Botswana results summary show that 3D-CCVNN prevails over other algorithms.

n	Metric	Bicubic	3D-FCNN[20]	3D-SRCNN[21]	3D-RUNET[22]	3D-CCVNN
x2	PSNR	32.83	32.95	33.14	33.34	**34.88**
	SSIM	0.873	0.905	0.912	0.914	**0.918**
	SAM	3.07	3.02	2.85	2.66	**2.38**
x4	PSNR	29.60	29.86	30.19	30.22	**31.20**
	SSIM	0.743	0.772	0.798	**0.811**	0.802
	SAM	4.74	4.70	4.45	4.43	**4.35**

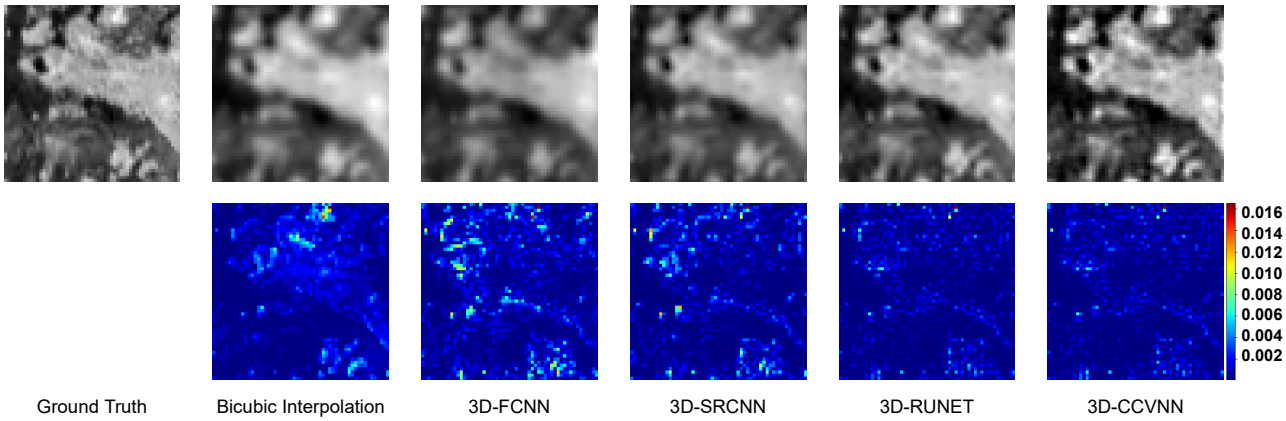

Figure 2. Qualitative results of Bicubic interpolation, 3D-FCNN, 3D-SRCNN, 3D-RUNET, and 3D-CVNN compared to the ground truth for scale factor $\times 2$ using Botswana dataset. The top row shows the predicted HR-HSI, and the bottom row shows a visualization of MSE between each predicted result and the ground truth.

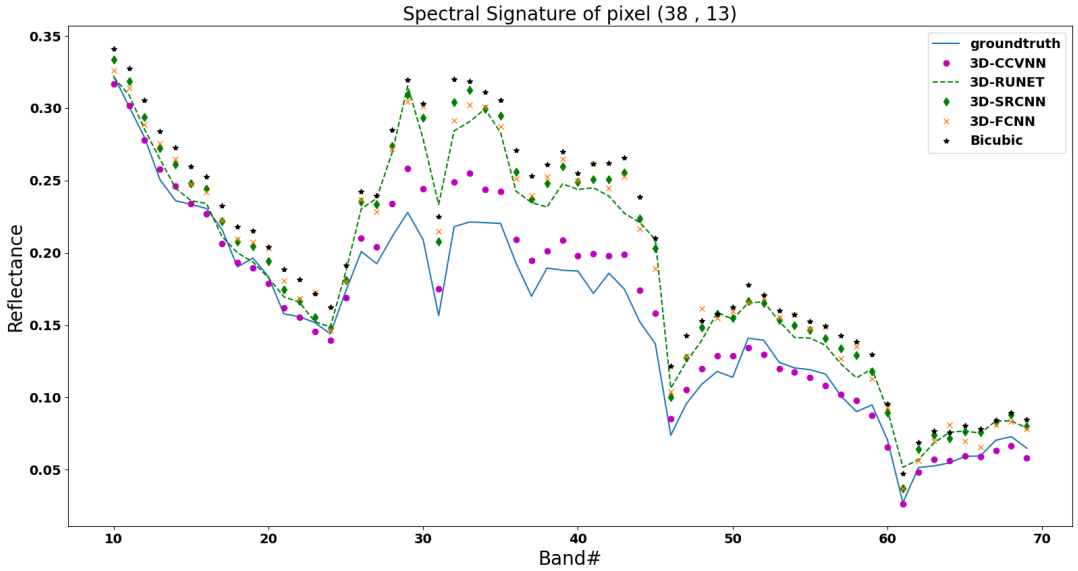

Figure 3. Spectral signature of a pixel taken at position (38,13) from Botswana dataset.

method. Furthermore, Figure 5 shows the spectral signature of the pixel at location (1,54) as predicted by each method. This plot further reveals that 3D-SRCNN and 3D-RUNET follow the ground truth more closely than 3D-CCVNN, although the difference seems marginal and the general pattern of the signature is similar.

Table 3. PU results summary.

n	Metric	Bicubic	3D-FCNN[20]	3D-SRCNN[21]	3D-RUNET[22]	3D-CCVNN
x2	PSNR	29.12	29.88	30.18	30.06	**31.77**
	SSIM	0.869	0.875	0.905	0.879	**0.912**
	SAM	6.38	5.94	**5.40**	5.45	5.56
x4	PSNR	25.23	26.44	27.56	27.14	**28.69**
	SSIM	0.712	0.723	0.756	0.744	**0.768**
	SAM	9.94	6.68	**6.54**	6.62	6.65

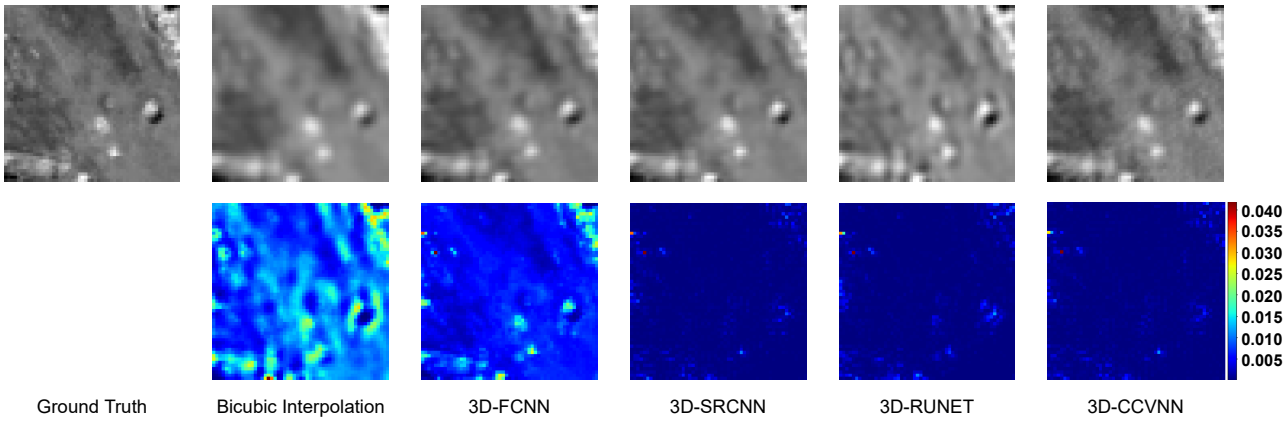

Figure 4. Qualitative results of Bicubic interpolation, 3D-FCNN, 3D-SRCNN, 3D-RUNET, and 3D-CVNN compared to the ground truth for scale factor ×2 using PU dataset. The top row shows the predicted HR-HSI, and the bottom row shows a visualization of MSE between each predicted result and the ground truth.

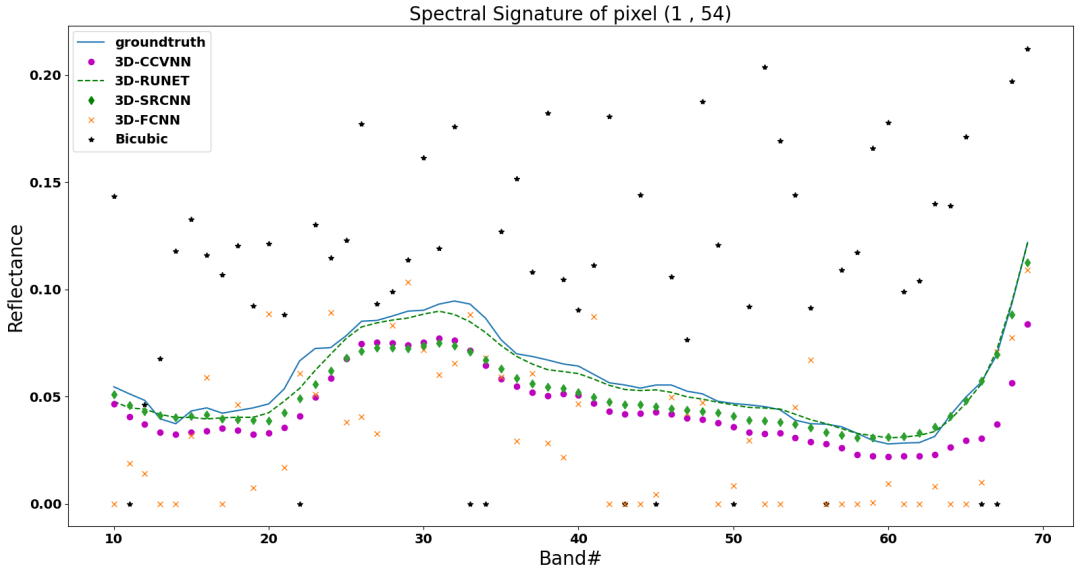

Figure 5. Spectral signature of a pixel taken at position (1, 54) from PU dataset.

5. CONCLUSION AND FUTURE DIRECTION

In this paper, a study on enhancing the spatial quality of HSI using 3D-CCVNN was conducted. The proposed network is analogous to the traditional 3D-SRCNN, which is known to perform well, with an additional residual connection and complex weights, operations, and activation function. FFT is used to transfer the HSI to the

complex domain, and the estimated HR-HSI is transferred back to the spatial domain using IFFT. The network is trained, tested, and evaluated using Botswana and PU datasets, and compared to other state-of-the-art methods. The results reveal that 3D-CCVNN can achieve a decent performance given a dataset of sufficient size. Most datasets available in the literature, such as PU, are of small size, which causes problems when training. The future direction of this research will tackle these problems. For example, the network may benefit from a complex loss function, as the one used in this paper is the standard MSE. Even though there are various cases in the literature where complex weights have been used with a real loss function, the benefit of a complex loss function is yet to be investigated. The degradation in SSIM, albeit slight, proves that the spatial context is important for the construction of the HR-HSI depending on the end purpose of the enhancement. Thus, mixing 2D and 3D layers within the complex network architecture may boost the performance. Finally, augmentation methods for HSI can be explored to increase the size of the dataset artificially.

REFERENCES

[1] Dong, C., Loy, C. C., He, K., and Tang, X., "Learning a deep convolutional network for image super-resolution," in [*Computer Vision – ECCV*], Fleet, D., Pajdla, T., Schiele, B., and Tuytelaars, T., eds., 184–199, Springer International Publishing, Cham (2014).

[2] Hu, X., Naiel, M. A., Wong, A., Lamm, M., and Fieguth, P., "RUNet: A robust UNet architecture for image super-resolution," in [*Proceedings of the IEEE/CVF Conference on Computer Vision and Pattern Recognition (CVPR) Workshops*], (June 2019).

[3] Aburaed, N., Panthakkan, A., III, S. A., and Al-Ahmad, H., "Super resolution of DS-2 satellite imagery using deep convolutional neural network," in [*Image and Signal Processing for Remote Sensing XXV*], Bruzzone, L. and Bovolo, F., eds., **11155**, 111551I, International Society for Optics and Photonics, SPIE (2019).

[4] Aburaed, N., Panthakkan, A., Al-Saad, M., Rai, M. C. E., Mansoori, S. A., Al-Ahmad, H., and Marshall, S., "Super-resolution of satellite imagery using a wavelet multiscale-based deep convolutional neural network model," in [*Image and Signal Processing for Remote Sensing XXVI*], Bruzzone, L., Bovolo, F., and Santi, E., eds., **11533**, 115331J, International Society for Optics and Photonics, SPIE (2020).

[5] Zhukov, B., Oertel, D., Lanzl, F., and Reinhackel, G., "Unmixing-based multisensor multiresolution image fusion," *IEEE Transactions on Geoscience and Remote Sensing* **37**(3), 1212–1226 (1999).

[6] Dong, W., Yang, Y., Qu, J., Xiao, S., and Du, Q., "Hyperspectral pansharpening via local intensity component and local injection gain estimation," *IEEE Geoscience and Remote Sensing Letters* **19**, 1–5 (2022).

[7] Vivone, G., Restaino, R., Dalla Mura, M., Licciardi, G., and Chanussot, J., "Contrast and error-based fusion schemes for multispectral image pansharpening," *IEEE Geoscience and Remote Sensing Letters* **11**(5), 930–934 (2014).

[8] Lin, C.-H., Ma, F., Chi, C.-Y., and Hsieh, C.-H., "A convex optimization-based coupled nonnegative matrix factorization algorithm for hyperspectral and multispectral data fusion," *IEEE Transactions on Geoscience and Remote Sensing* **56**(3), 1652–1667 (2018).

[9] Guo, S., Chen, X., Jia, H., Han, Z., Duan, Z., and Tang, Y., "Fusing hyperspectral and multispectral images via low-rank hankel tensor representation," *Remote Sensing* **14**(18) (2022).

[10] Liu, H., Jiang, W., Zha, Y., and Wei, Z., "Coupled tensor block term decomposition with superpixel-based graph laplacian regularization for hyperspectral super-resolution," *Remote Sensing* **14**(18) (2022).

[11] Wei, Q., Bioucas-Dias, J., Dobigeon, N., and Tourneret, J., "Hyperspectral and multispectral image fusion based on a sparse representation," *IEEE Transactions on Geoscience and Remote Sensing* **53**(7), 3658–3668 (2015).

[12] Simões, M., Bioucas-Dias, J., Almeida, L. B., and Chanussot, J., "Hyperspectral image superresolution: An edge-preserving convex formulation," in [*IEEE International Conference on Image Processing (ICIP)*], 4166–4170 (2014).

[13] Prévost, C., Chainais, P., and Boyer, R., "Fast fusion of hyperspectral and multispectral images: A tucker approximation approach," in [*2022 IEEE International Conference on Image Processing (ICIP)*], 2076–2080 (2022).

[14] Bhattacharya, S., Remane, K., Kindel, B., and Tang, G., "Spectral super-resolution for hyperspectral image reconstruction using dictionary and machine learning," in [*IEEE International Geoscience and Remote Sensing Symposium*], 1764–1767 (2022).

[15] Wang, X., Wang, X., Zhao, K., Zhao, X., and Song, C., "Fsl-unet: Full-scale linked unet with spatial–spectral joint perceptual attention for hyperspectral and multispectral image fusion," *IEEE Transactions on Geoscience and Remote Sensing* **60**, 1–14 (2022).

[16] Huang, S. and Messinger, D. W., "An unsupervised laplacian pyramid network for radiometrically accurate data fusion of hyperspectral and multispectral imagery," *IEEE Transactions on Geoscience and Remote Sensing* **60**, 1–17 (2022).

[17] Ha, V. K., Ren, J., Wang, Z., Sun, G., Zhao, H., and Marshall, S., "Multiscale spatial fusion and regularization induced unsupervised auxiliary task cnn model for deep super-resolution of hyperspectral images," *IEEE Journal of Selected Topics in Applied Earth Observations and Remote Sensing* **15**, 4583–4598 (2022).

[18] Wang, Z., Chen, B., Zhang, H., and Liu, H., "Unsupervised hyperspectral and multispectral images fusion based on nonlinear variational probabilistic generative model," *IEEE Transactions on Neural Networks and Learning Systems* **33**(2), 721–735 (2022).

[19] Graña, M., Veganzons, M., and Ayerdi, B., "Hyperspectral Remote Sensing Scenes." 12 July 2021 https://www.ehu.eus/ccwintco/index.php/Hyperspectral_Remote_Sensing_Scenes. (Accessed: 20 November 2022).

[20] Mei, S., Yuan, X., Ji, J., Zhang, Y., Wan, S., and Du, Q., "Hyperspectral image spatial super-resolution via 3d full convolutional neural network," *Remote Sensing* **9**(11) (2017).

[21] Aburaed, N., Alkhatib, M. Q., Marshall, S., Zabalza, J., and Al Ahmad, H., "3d expansion of srcnn for spatial enhancement of hyperspectral remote sensing images," in [*2021 4th International Conference on Signal Processing and Information Security (ICSPIS)*], 9–12 (2021).

[22] Aburaed, N., Alkhatib, M. Q., Marshall, S., Zabalza, J., and Ahmad, H. A., "Sisr of hyperspectral remote sensing imagery using 3d encoder-decoder runet architecture," in [*IGARSS 2022 - 2022 IEEE International Geoscience and Remote Sensing Symposium*], 1516–1519 (2022).

[23] Liu, W. and Lee, J., "An efficient residual learning neural network for hyperspectral image superresolution," *IEEE Journal of Selected Topics in Applied Earth Observations and Remote Sensing* **12**(4), 1240–1253 (2019).

[24] Wang, L., Bi, T., and Shi, Y., "A frequency-separated 3D-CNN for hyperspectral image super-resolution," *IEEE Access* **8**, 86367–86379 (2020).

[25] Dou, X., Li, C., Shi, Q., and Liu, M., "Super-resolution for hyperspectral remote sensing images based on the 3d Attention-SRGAN network," *Remote Sensing* **12**(7) (2020).

[26] Li, Y., Zhang, L., Dingl, C., Wei, W., and Zhang, Y., "Single hyperspectral image super-resolution with grouped deep recursive residual network," in [*IEEE 4th International Conference on Multimedia Big Data (BigMM)*], 1–4 (2018).

[27] Ingram, R. N., Lewis, A. S., and Tutwiler, R. L., "An automatic nonlinear correlation approach for processing of hyperspectral images," *International Journal of Remote Sensing* **25**(22), 4981–4998 (2004).

[28] Lim, B., Son, S., Kim, H., Nah, S., and Lee, K. M., "Enhanced deep residual networks for single image super-resolution," *CoRR* **abs/1707.02921** (2017).